

Unusual Phonon Thermal Transport Mechanisms in Monolayer Beryllene

Sapta Sindhu Paul Chowdhury  and Santosh Mogurampelly ^{*}

*Department of Physics, Indian Institute of Technology Jodhpur
N.H. 62, Nagaur Road, Karwar, Jodhpur, Rajasthan, India - 342030.*

(Dated: September 10, 2024)

We compute the thermal conductivity of monolayer beryllene using the linearized phonon Boltzmann transport equation with interatomic force constants obtained from *ab-initio* calculations. Monolayer beryllene exhibits an impressive thermal conductivity of 270 W/m·K at room temperature, exceeding that of bulk beryllium by over 100%. Our study reveals a remarkable temperature-dependent behavior: $\kappa \sim T^{-2}$ at low temperatures, attributed to higher normal phonon-phonon scatterings, and $\kappa \sim T^{-1}$ at high temperatures due to Umklapp phonon interactions. Mode-specific analysis reveals that flexural phonons with longer lifetimes are the primary contributors to thermal conductivity, accounting for approximately 80%. This dominance results from their lower scattering rates in the out-of-plane direction due to a restricted phase space for scattering processes. Additionally, our findings highlight suppressed Umklapp scattering and reduced phase space for flexural modes, providing a thorough understanding of the eased thermal conductivity in monolayer beryllene and its potential for advanced thermal management applications.

Monolayer beryllene (α -beryllene) is the lightest known two-dimensional (2D) material, featuring a structure similar to graphene but with an even lower atomic mass [1]. While extensive studies on the thermal transport in 2D materials like graphene have provided deep insights into their electronic and phononic behavior [2], similar investigations into α -beryllene are still in their infancy. Graphene's exceptional thermal conductivity and the well-characterized mechanisms of heat transport serve as a benchmark, yet the thermal transport properties of α -beryllene remain largely unexplored [3].

Recent progress, including the theoretical prediction and successful experimental synthesis of α -beryllene, has sparked interest in its unique properties and potential applications [1, 4]. Beryllium, known for its impressive thermal properties, has a specific heat capacity of approximately 1.82 J/g·K at room temperature [5], a low thermal expansion coefficient of about $16.8 \times 10^{-6} \text{ K}^{-1}$ [6], and a high thermal conductivity of around 115 W/m·K [7]. These properties position beryllium as a strong candidate for high-performance thermal management and precision applications. Given these outstanding thermal properties of beryllium, it is reasonable to anticipate that its two-dimensional counterpart, α -beryllene, would exhibit significant potential in thermal management and energy storage applications. Indeed, monolayer beryllene is stable up to 1500 K, and its metallic nature suggests considerable promise for use in metal-ion batteries [8]. Additionally, α -beryllene has demonstrated superconductivity with a transition temperature of 9.9 K, a property linked to its in-plane covalent bonds and distinctive vibrational modes [9]. Furthermore, Ghavami et al. explored its application in beryllene/graphene/beryllene trilayer heterostructures for optoelectronic devices, revealing transitions from non-convex to hyperbolic plasmonic regions [10]. Despite these promising advances, a detailed understanding of the thermal conductivity of α -beryllene

remains limited.

Investigating the thermal conductivity of α -beryllene and unraveling the mechanisms of heat transport is critical for several reasons. High thermal conductivity in 2D materials is critical not only for thermal management but also for their electronic and mechanical performance. The unique properties of α -beryllene, coupled with its potential for use in advanced thermal management and optoelectronic devices, emphasize the necessity of thoroughly understanding its thermal transport characteristics.

In this work, motivated by the above discussed lacunas, we use *ab-initio* density functional theory (DFT) to calculate the phonon thermal conductivity of monolayer beryllene and examine the underlying heat transport mechanisms in detail. We use the plane wave basis set based formulations of DFT *quantum espresso* [11, 12] with the Perdew–Burke–Ernzerhof functional [13] and norm-conserving pseudopotential [14] to calculate the ground state solution for α -beryllene. To accurately model the phonons, a high plane wave kinetic energy cutoff of 80 Ry with a dual of 4 is used. The Hellmann-Feynman forces and the total energy are minimized with a tolerance of 10^{-8} eV/\AA and 10^{-10} eV , respectively. A dense Monkhorst-Pack [15] k-point mesh of $72 \times 72 \times 1$ is used with a Marzari-Vanderbilt smearing [16] of 0.01 eV in the self-consistent calculations. A 25 Å vacuum is introduced along the z-direction to eliminate interactions between adjacent α -beryllene layers due to periodic boundary conditions. We use the highly accurate density functional perturbation theory to calculate the harmonic phonons with a converged q point mesh of $24 \times 24 \times 1$ as the phonon dispersion may not be accurate for the acoustic bands with the finite difference method [17]. Finite displacement method with a supercell of $8 \times 8 \times 1$, and 7 nearest neighbors are used to estimate the anharmonic interatomic force constants [18].

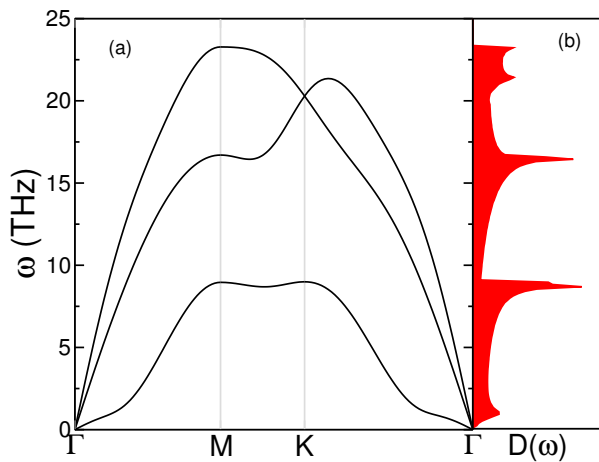


FIG. 1. (a) Phonon dispersion and (b) phonon density of states for monolayer beryllene, calculated using density functional perturbation theory. The absence of optical modes, with only acoustic phonon branches present, reflects the monatomic nature of the beryllene monolayer.

The monolayer structure of beryllene exhibits a distinctive hexagonal planar configuration with six first nearest neighbors, characterized by a lattice constant of 2.13 Å. This structure belongs to the P6/mmm space group and D_{6h} point group symmetry, consistent with earlier theoretical predictions and experimental observations [1, 4]. We systematically optimize the phonon frequencies by adjusting the kinetic energy cutoffs as the precision of phonon dispersion is critical for accurate thermal conductivity calculations. We show the phonon dispersion relations plotted along the high-symmetry directions $\Gamma \rightarrow M \rightarrow K \rightarrow \Gamma$ in Fig. 1(a). We find a maximum phonon frequency of 23.4 THz at the Γ point consistent with prior studies [4, 9] confirming the validity and accuracy of our computational methods.

The phonon spectrum consists exclusively of acoustic modes, specifically the out-of-plane acoustic (ZA) mode and the in-plane transverse acoustic (TA) and longitudinal acoustic (LA) modes due to the monatomic nature of beryllene. The absence of any soft phonon modes indicates the dynamical stability of α -beryllene. The flexural ZA mode displays a characteristic quadratic behavior, while the in-plane TA and LA modes exhibit cubic behavior, analogous to that of graphene [19]. The quadratic dispersion of the ZA mode can be attributed to the layer bending stiffness, a phenomenon well-explained by the elastic plate theory, while the cubic behavior of the in-plane modes is a result of in-plane stretching vibrations [20]. The sharp features in the phonon density of states (Fig. 1(b)) correspond to saddle points at the M and K points in the Brillouin zone, highlighting the complex vibrational landscape of this material.

We calculate the thermal conductivity of beryllene monolayer by solving the linearized Boltzmann transport

equation (LBTE) on a $72 \times 72 \times 1$ grid with the conjugate gradient method [21]. The lattice thermal conductivity tensor in the $\alpha\beta$ -direction is given by:

$$\kappa_L^{\alpha\beta} = \frac{\hbar^2}{k_B T^2 \Omega N_0} \sum_{\mathbf{q}j} \omega_{\mathbf{q}j}^2 \bar{n}_{\mathbf{q}j} (\bar{n}_{\mathbf{q}j} + 1) (v_{\mathbf{q}j}^\alpha + \Delta_{\mathbf{q}j}^\alpha) \times (v_{\mathbf{q}j}^\beta + \Delta_{\mathbf{q}j}^\beta) \tau_{\mathbf{q}j},$$

where k_B is the Boltzmann constant, Ω the volume of unit cell, N_0 the number of q -points in the first Brillouin zone, \hbar the reduced Planck's constant, $\bar{n}_{\mathbf{q}j}$ is the Bose-Einstein distribution function for the phonon population of $\mathbf{q}j$ mode at temperature T , with frequency $\omega_{\mathbf{q}j}$. The volume Ω is calculated using the thickness of the α -beryllene sheet as 3.06 Å, the van der Waals diameter of Be atom. The group velocity is given by $v_{\mathbf{q}j}^\alpha (= d\omega_{\mathbf{q}j}/dq_\alpha)$ for a direction α . The terms $\Delta_{\mathbf{q}j}^\alpha$ and $\Delta_{\mathbf{q}j}^\beta$ arise from the exact solution of the LBTE, which corrects the inaccuracies of the relaxation time ($\tau_{\mathbf{q}j}$) approximation. More details on this are available in the Supplemental Material S1.

The thermal conductivity is found to be 270 W/m·K at room temperature, which is more than double its counterpart bulk beryllium [7], signifying a superior thermal transport in α -beryllene. This increase can be attributed to α -beryllene's planar atomic structure, which minimizes anharmonic phonon interactions and increases phonon mean free path (MFP), thereby enhancing its thermal conductivity. This behavior is in sharp contrast to that of buckled 2D materials such as silicene and germanene, where the presence of out-of-plane distortions leads to increased phonon scattering and lower thermal

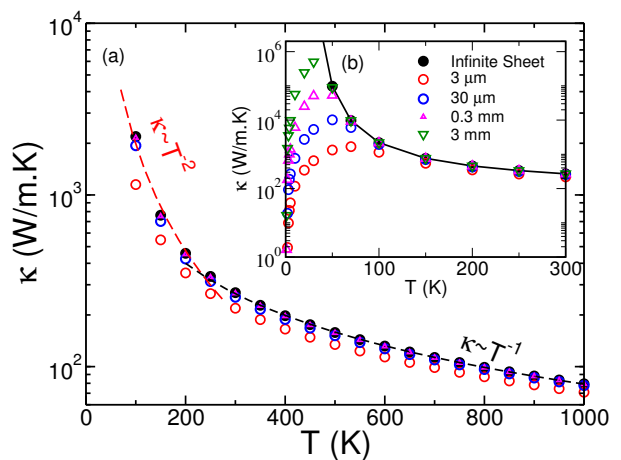


FIG. 2. (a) Temperature-dependent thermal conductivity of monolayer beryllene, calculated using the exact solution of the LBTE. (b) Zoomed-in view of the low-temperature regime, highlighting the significant variation in thermal conductivity due to boundary scattering effects for finite sample size. In this regime, thermal conductivity diverges for a periodic lattice with infinite length.

conductivity [22–24]. However, planar 2D materials such as graphene and h-BN show increased thermal conductivity due to reduced dimensionality and strong in-plane bonding. It must be noted that while the \mathcal{L} BTE diverges with an iterative solver, it successfully converges when employing the variational principle with a conjugate gradient solver, as previously observed in diamond [21]. This divergence can be attributed to the higher prevalence of normal (N) scattering processes compared to Umklapp (U) scatterings, even at high temperatures as illustrated in Fig. S1.

In Fig. 2(a), we present the variation of thermal conductivity with temperature. We find a unusual $\kappa \sim T^{-2}$ dependency at low and $\kappa \sim T^{-1}$ at high temperatures, diverting from the ideal $\kappa \sim T^{-1}$ behavior. Notably, for a periodic sheet of infinite length, the thermal conductivity (κ) diverges at lower temperatures ($T < 100$ K). This divergence arises due to the idealized nature of the infinite sheet, where boundary scattering is absent, leading to an unusual increase in thermal conductivity as temperature decreases. However, when considering finite sample sizes (Fig. 2(b)) found in realistic experimental conditions, the thermal conductivity behaves differently; κ converges due to the presence of boundary scattering, which limits the MFPs of phonons. Thermal conductivity increases steadily with temperature and peaks in between 80-100 K depending on the grain size. With a further increase in temperature, the thermal conductivity decreases monotonically. This contrast between infinite and finite systems emphasizes the critical role of sample size in thermal transport. The divergence observed in infinite sheets highlights the theoretical limit of thermal conductivity in an ideal lattice, a condition that is practically unattainable in experiments due to the inherent challenges in isolating an infinitely long monolayer sheet. Therefore, the finite sample size calculations provide a more realistic and intuitive understanding of how grain size and boundary effects influence the thermal conductivity of α -beryllene.

To gain deeper insights, we plot the normalized accumulated thermal conductivity of an infinitely long α -beryllene sheet as a function of MFPs at room temperature in Fig. 3(a). Our results demonstrate a clear convergence of thermal conductivity beyond $30 \mu\text{m}$, indicating that phonons with MFPs longer than this contribute negligibly to thermal transport. Strikingly, approximately 50% of the total thermal conductivity originates from phonons with MFPs shorter than 100 nm, while nearly 90% is contributed by phonons with MFPs below 1000 nm. This indicates that the majority of heat transport in α -beryllene is dominated by phonons with relatively short MFPs, highlighting the significance of boundary scattering and the finite size effects in this material. We also calculate the normalized accumulated thermal conductivity as a function of phonon angular frequency, as shown in Fig. 3(b). We find that low- and mid-frequency

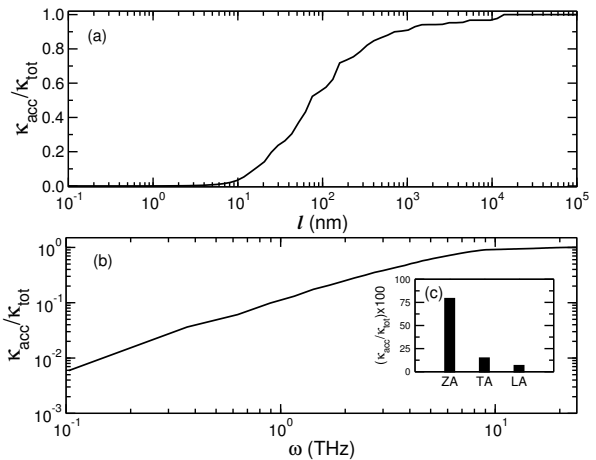


FIG. 3. (a) The normalized accumulated thermal conductivity of monolayer beryllene at room temperature as a function of phonon MFP, (b) the accumulated thermal conductivity as a function of phonon angular frequency, and (c) the percentage contribution to the total thermal conductivity from different phonon modes. It is observed that flexural modes account for approximately 80% of the thermal conductivity in the system.

phonons (1-10 THz) are the primary carriers of heat energy in α -beryllene, accounting for approximately 80% of the total accumulated thermal conductivity. The remaining 20% is almost equally divided between ultra-low frequency phonons (0-1 THz) and high-frequency phonons (10-24 THz).

A detailed examination of the contribution from different phonon branches reveals an even more intricate picture. The low frequency phonon branch, corresponding to the flexural ZA phonons, contributes a remarkable 80% of the total thermal conductivity at room temperature. This dominance of ZA phonons is indicative of the significant role of flexural modes in the thermal transport of two-dimensional (2D) materials, where the reduced dimensionality enhances the contribution of out-of-plane

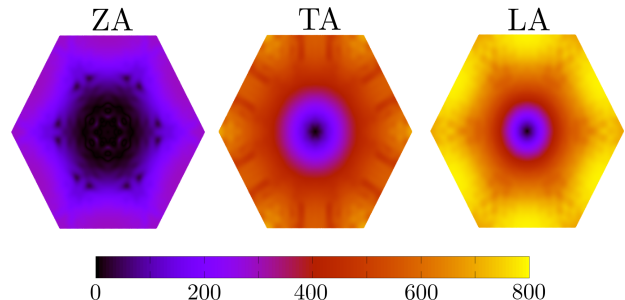


FIG. 4. Phonon linewidths (in cm^{-1}) of different phonon modes projected across the first Brillouin zone. The ZA modes exhibit the lowest linewidths, with a maximum of approximately 300 cm^{-1} , indicating a longer phonon lifetime for the ZA modes.

vibrations. In stark contrast, the in-plane TA and LA branches contribute only 12% and 6% to the total thermal conductivity, respectively. These results strongly reinforce the widely recognized consensus in the literature that flexural phonons are the predominant heat carriers in 2D materials [25].

In Fig. 4, we show the phonon linewidth, which is the inverse of phonon lifetime. We find that the ZA phonons exhibit the lowest linewidth, with a maximum value of 300 cm^{-1} . In contrast, the in-plane phonon modes display significantly higher linewidths, with TA modes reaching up to 700 cm^{-1} and LA modes up to 800 cm^{-1} . A lower linewidth corresponds to reduced phonon scattering and, consequently, a longer phonon lifetime. This observation strongly suggests that ZA phonons have the longest lifetimes among the phonon branches, which directly correlates with their substantial contribution to the overall thermal conductivity. The low scattering rates and extended lifetimes of ZA phonons can be attributed to the high symmetry of the system, which prohibits a number of scattering processes. In α -beryllene, third-order force constants involving an odd number of flexural components vanish due to reflection symmetry. As a result, scattering processes that involve one and three out-of-plane modes, such as $\text{ZA} + \text{LA} \rightarrow \text{TA}$ and $\text{ZA} + \text{ZA} \rightarrow \text{ZA}$, are forbidden [19, 26] resulting in lower total scatterings and a increase in the thermal conductivity.

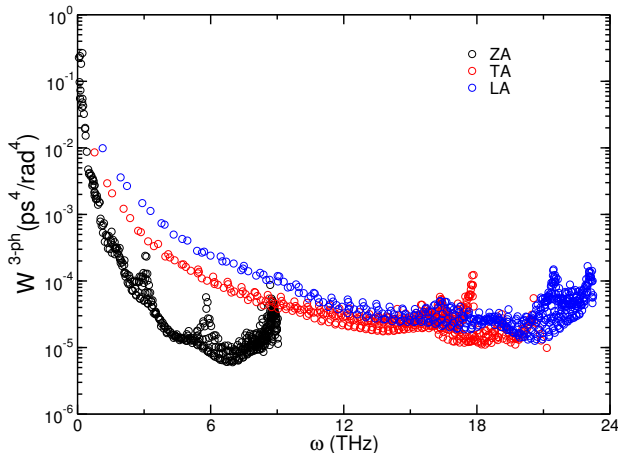


FIG. 5. The weighted phase space volume available for anharmonic three-phonon scattering as a function of angular frequency. The ZA modes exhibit lower scattering due to the reduced phase space volume accessible to ZA phonons compared to other phonon modes.

To further elucidate these findings, we plotted the weighted phase space available for three-phonon anharmonic scattering processes against the phonon angular frequencies (Fig. 5). The analysis indicates that ZA phonons have significantly less phase space available for scattering compared to in-plane modes. This limited phase space in the flexural direction severely restricts

the number of allowed scattering processes, thereby contributing to the dominant role of ZA phonons in thermal transport and a significant increase in thermal conductivity in beryllene.

The role of N scattering processes where momentum is conserved, is remarkably significant in α -beryllene (Fig. S1). In the case of α -beryllene the planar structure inherently promotes these momentum-conserving interactions making N scatterings a dominant mechanism, particularly in the low-temperature regime. This results in a unusual $\kappa \sim T^{-2}$ dependency at lower temperatures. This dominance of N scatterings can be attributed to the reduced phase space available for U processes at lower temperatures, where thermal excitation is insufficient to overcome the energy barriers required for significant U scattering. Consequently, the phonons in α -beryllene, especially those associated with flexural modes, experience less resistive scattering, allowing for elevated ballistic transport and higher thermal conductivity at these lower temperatures. Moreover, the 2D monatomic nature of α -beryllene enhances this effect by limiting the number of available scattering channels and further suppressing U interactions. This insight not only deepens our understanding of the fundamental thermal transport mechanisms in α -beryllene but also highlights the broader implications for designing and optimizing other 2D materials with similar structural characteristics [2, 27]

In conclusion, our *ab-initio* investigation of monolayer beryllene reveal an exceptional thermal conductivity of $270 \text{ W/m}\cdot\text{K}$ at room temperature, more than twice that of its bulk counterpart. The short-wavelength phonons with MFPs less than 100 nm contribute to half of the total thermal conductivity and 90% of the thermal conductivity arises from phonons with frequencies below 10 THz . The out-of-plane ZA phonons dominates rule with contribution of approximately 80% of the total thermal conductivity as a result of reduced phase space availability due to planer nature of beryllene. We uncover an unusual $\kappa \sim T^{-2}$ temperature-dependent scaling behavior of thermal conductivity observed at low temperatures due to dominant N-scatterings and higher ballistic phonon transport. The usual $\kappa \sim T^{-1}$ at higher temperatures indicates an increase in U phonon-phonon interactions. Our findings demonstrate that α -beryllene is an excellent thermal conductor at room temperature with potential for applications in thermal interfacing devices. Given its unique thermal transport mechanisms, further experimental and theoretical research into α -beryllene are a must for designing advanced thermal management devices .

The authors acknowledge the Computer Center of IIT Jodhpur for providing computing resources that have contributed to the research results reported in this paper. SSPC acknowledges the Ministry of Education (MoE), Govt. of India, for partial financial support received as a fellowship.

* santosh@iitj.ac.in

- [1] S. Chahal, A. Bandyopadhyay, C.-S. Yang, and P. Kumar, *npj 2D Materials and Applications* **7**, 55 (2023).
- [2] X. Gu, Y. Wei, X. Yin, B. Li, and R. Yang, *Rev. Mod. Phys.* **90**, 041002 (2018).
- [3] M. Sang, J. Shin, K. Kim, and K. J. Yu, *Nanomaterials* **9** (2019), 10.3390/nano9030374.
- [4] M. Sun, Y. Yan, and U. Schwingenschlöggl, *The Journal of Physical Chemistry Letters* **11**, 9051 (2020), pMID: 33044084, <https://doi.org/10.1021/acs.jpcclett.0c02426>.
- [5] D. C. Ginnings, T. B. Douglas, and A. F. Ball, *Journal of the American Chemical Society* **73**, 1236 (1951), <https://doi.org/10.1021/ja01147a107>.
- [6] P. Hidnert and W. T. Sweeney, *Scientific Papers of the Bureau of Standards* **22**, 533–545 (1927).
- [7] R. Powell, *The London, Edinburgh, and Dublin Philosophical Magazine and Journal of Science* **44**, 645 (1953), <https://doi.org/10.1080/14786440608521043>.
- [8] Q. Gao, X.-J. Ye, and C.-S. Liu, *Phys. Chem. Chem. Phys.* **25**, 6519 (2023).
- [9] J. Li, M. Guo, J. Si, L. Shi, X. Shi, J.-J. Ma, Q. Zhang, D. J. Singh, P.-F. Liu, and B.-T. Wang, *Materials Today Physics* **38**, 101257 (2023).
- [10] B. Ghavami, E. Rostampour, and C. Stampfl, *Optik* **300**, 171690 (2024).
- [11] P. Giannozzi, S. Baroni, N. Bonini, M. Calandra, R. Car, C. Cavazzoni, D. Ceresoli, G. L. Chiarotti, M. Cococcioni, I. Dabo, A. D. Corso, S. Fabris, G. Fratesi, S. de Gironcoli, R. Gebauer, U. Gerstmann, C. Gougousis, A. Kokalj, M. Lazzeri, L. Martin-Samos, N. Marzari, F. Mauri, R. Mazzarello, S. Paolini, A. Pasquarello, L. Paulatto, C. Sbraccia, S. Scandolo, G. Sclauzero, A. P. Seitsonen, A. Smogunov, P. Umari, and R. M. Wentzcovitch, *J. Phys. Condens. Matter* **21**, 395502 (2009).
- [12] P. Giannozzi, O. Andreussi, T. Brumme, O. Bunau, M. B. Nardelli, M. Calandra, R. Car, C. Cavazzoni, D. Ceresoli, M. Cococcioni, N. Colonna, I. Carnimeo, A. D. Corso, S. de Gironcoli, P. Delugas, R. A. D. Jr, A. Ferretti, A. Floris, G. Fratesi, G. Fugallo, R. Gebauer, U. Gerstmann, F. Giustino, T. Gorni, J. Jia, M. Kawamura, H.-Y. Ko, A. Kokalj, E. Kucukbenli, M. Lazzeri, M. Marsili, N. Marzari, F. Mauri, N. L. Nguyen, H.-V. Nguyen, A. O. de-la Roza, L. Paulatto, S. Ponce, D. Rocca, R. Sabatini, B. Santra, M. Schlipf, A. P. Seitsonen, A. Smogunov, I. Timrov, T. Thonhauser, P. Umari, N. Vast, X. Wu, and S. Baroni, *J. Phys. Condens. Matter* **29**, 465901 (2017).
- [13] J. P. Perdew, K. Burke, and M. Ernzerhof, *Phys. Rev. Lett.* **77**, 3865 (1996).
- [14] G. Prandini, A. Marrazzo, I. E. Castelli, N. Mounet, and N. Marzari, *npj Computational Materials* **4**, 72 (2018), <http://materialscloud.org/sssp>.
- [15] H. J. Monkhorst and J. D. Pack, *Phys. Rev. B* **13**, 5188 (1976).
- [16] N. Marzari, D. Vanderbilt, A. De Vita, and M. C. Payne, *Phys. Rev. Lett.* **82**, 3296 (1999).
- [17] A. J. H. McGaughey, A. Jain, H.-Y. Kim, and B. Fu, *Journal of Applied Physics* **125**, 011101 (2019).
- [18] W. Li, L. Lindsay, D. A. Broido, D. A. Stewart, and N. Mingo, *Phys. Rev. B* **86**, 174307 (2012).
- [19] X. Gu and R. Yang, *Journal of Applied Physics* **117**, 025102 (2015).
- [20] H. Zabel, *Journal of Physics: Condensed Matter* **13**, 7679 (2001).
- [21] G. Fugallo, M. Lazzeri, L. Paulatto, and F. Mauri, *Phys. Rev. B* **88**, 045430 (2013).
- [22] S. S. Paul Chowdhury, A. Samudrala, and S. Mogurampelly, *Phys. Rev. B* **108**, 155436 (2023).
- [23] S. Thapliyal, S. S. Paul Chowdhury, and S. Mogurampelly, in *Energy Materials and Devices*, edited by A. Dixit, V. K. Singh, and S. Ahmad (Springer Nature Singapore, Singapore, 2024) pp. 325–335.
- [24] H. Gholivand and N. Donmez, *IEEE Transactions on Nanotechnology* **16**, 752 (2017).
- [25] H. Xie, T. Ouyang, E. Germaneau, G. Qin, M. Hu, and H. Bao, *Phys. Rev. B* **93**, 075404 (2016).
- [26] L. Lindsay, D. A. Broido, and N. Mingo, *Phys. Rev. B* **82**, 115427 (2010).
- [27] L. Lindsay and D. A. Broido, *Phys. Rev. B* **81**, 205441 (2010).